JOURNAL OF CATALYSIS 57, 236–252 (1979)

Some Selectivity Criteria in Mild Oxidation Catalysis

V–P–O Phases in Butene Oxidation to Maleic Anhydride

E. BORDES AND P. COURTINE

Département de Génie Chimique, Université de Technologie de Compiègne, B. P. 233, 60206 Compiègne, France

Received October 14, 1977; revised July 20, 1978

The V–P–O system, active and selective in the oxidation of butene into maleic anhydride, provides an additional example of a mild oxidation catalyst, where the catalytic properties are shown to depend strongly on the intrinsic properties of the constituent phases. The structural and spectroscopic properties of $VOPO_4$ and $(VO)_2P_2O_7$, whose presence is necessary to obtain a substantial selectivity in the range P:V = 0.5:1 to 2:1, have been examined in connection with those of V_2O_5. Since electron diffraction patterns obtained on spent catalyst samples revealed the existence of microdomains, these results have been compared with the hysteresis loop found in kinetic and thermodynamic experiments: The excited atoms, which are located on each side of the coherent boundaries formed in steady state conditions, are assumed to influence strongly the activity and selectivity.

I. INTRODUCTION

For fundamental and applied reasons, the need for a greater emphasis on the problem of selectivity in mild oxidation heterogeneous catalysis is now unanimously recognized. A survey of recent literature indicates that experimental work is being conducted with this in mind (*1, 2*).

Up to now, whereas catalytic activity is generally explained either by considering the metal–oxygen bond strength (*3–5*), or by the role played by oxygen species on the catalyst surface (*6–8*), correlations with selectivity are still difficult to establish, in spite of encouraging attempts (*9, 10*).

Since a selective catalyst is generally composed of two oxides, one being responsible for activity and the other giving rise to selectivity (*2, 11*), some authors correlate the latter property with the presence of certain ions in appropriate coordination acting as catalytic sites, rather than to the existence of defined phases present in the catalyst. In the same way, others establish a direct relationship between one property of the active ions (such as acidity) and their selectivity, as if it were a more or less additive function of the composition of the binary catalyst (*10*).

However, it has been frequently observed that the same active ions behave differently according to their crystalline environment, exhibiting various selectivities in the same gas phase reaction. Electron transfer and electronic interactions with ions in adjacent polyhedra are responsible for this behavior, providing the so-called "localized approach" to the problem of catalytic centers already extensively studied (*12, 13*). It means that any correlation must take into account not only the free active ions with their intrinsic properties, but also the same ions in their solid state environment, which results from the short

0021-9517/79/050236-17$02.00/0

TABLE 1

Various Methods for the Preparation of P:V = 1:1 Catalysts

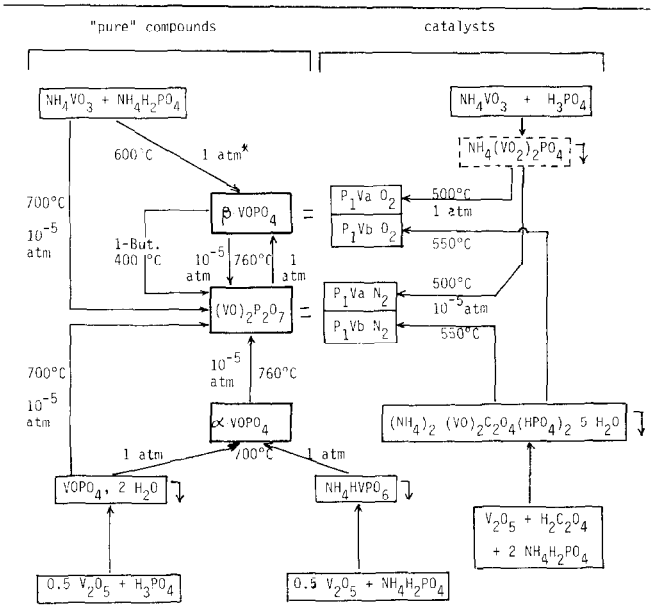

* Temperature of calcination and pressure of oxygen.

or long range crystalline field around them. Therefore, a study of the interdependent properties of the crystalline matrix, which gives the active ions their specificity, appears to be the first step necessary to obtain selectivity criteria.

Considering the oxidation of 1-butene into maleic anhydride (MAA), the behavior of the V^{5+}/V^{4+} redox couple has been studied in comparing the properties of the well-known V_2O_5 catalyst and those of the V–P–O system, which is not yet fully understood though already industrially used in this reaction (*2*). Given the close relationships between the two catalysts, it has been thought that any difference in the catalytic selectivity of V–P–O as compared to that of V_2O_5 could be easily interpreted in terms of its specific properties. Moreover, since P:V = 1:1 and 1.6:1 (atomic ratio) catalysts are equally selective in first approximation (*14*), this system provides the opportunity to point out the role of thermodynamically defined phases in mild oxidation catalysts.

II. METHODS

A. Preparation of Catalysts

The catalysts have been prepared by precipitation from solution or evaporation to dryness, then drying in an oven at 110°C and calcination under gas flow (1 liter hr^{-1}) at a moderate temperature (450–550°C) (Table 1).

(a) NH_4VO_3 (0.25 mole) was partly dissolved in 250 ml of hot water while stirring at 60°C, then 85 wt% H_3PO_4 (stoichiometric amounts) was added. After a fleeting, intense reddish brown coloration, the yellow compound $NH_4(VO_2)_2PO_4$ precipitated. The whole mixture was evaporated to dryness with constant stirring and dried at 110°C for 8 hr. The yellow pre-

cursor so obtained was heated for 4 hr under flowing nitrogen ($pO_2 = 10^{-5}$ atm O_2), air or oxygen, at 500°C (catalysts $P_{0.5}Va$,[1] P_1Va, $P_{1.6}Va$, P_2Va).

(b) V_2O_5 (0.1 mole) was dissolved in 150 ml of a hot oxalic acid solution (0.5 mole). $NH_4H_2PO_4$ was added in stoichiometric proportions. For P:V = 1:1 catalyst, the green precipitate of $(NH_4)_2 \cdot [(VO)_2C_2O_4(HPO_4)_2] \cdot 5H_2O$ may be filtered after cooling, washed with water, and dried with acetone as in Ref. (*15*). The calcination under O_2, air, or N_2 at 550°C (5 hr) yields P_1Vb. The other P:V ratios could be obtained by evaporation of the whole mixture (solution and precipitate) and calcination in the same conditions ($P_{0.5}Vb$, $P_{1.6}Vb$, $P_{1.8}Vb$).

(c) V_2O_5 (0.02 mole) was added to a boiling solution of $NH_4H_2PO_4$ (0.4 mole in 300 ml H_2O), and boiling was maintained for 30 min. The yellow precipitate NH_4HVPO_6 obtained (*16*) was washed with water, dried with acetone, and calcined under O_2 at 550°C (P_1Vc).

(d) $VOPO_4$ was obtained by decomposition at 700°C under O_2 of $VOPO_4 \cdot 2H_2O$, prepared as described by Ladwig (*17*).

(e) The solid precursors (NH_4VO_3 or V_2O_5 and $NH_4H_2PO_4$) were powdered and mixed in stoichiometric proportions. The calcination of P:V = 1:1 mixing yielded, respectively, β-$VOPO_4$ under O_2 and $(VO)_2P_2O_7$ under N_2 (600°C); $VO(PO_3)_2$ was obtained only if the calcination was performed under O_2 (P:V = 2:1).

As far as possible, the precursors dried at 110°C were broken into 5 to 10 mesh irregularly shaped pieces before calcination. If not, the catalysts were supported on Al_2O_3 beads (Norton Company, ϕ = 48 mm): After the calcination, the powdered catalyst was damped in a small amount of water; the paste obtained was put into motion in a disk granulator together with beads (e.g., about 35 g beads for 6 g catalyst) and dried quickly.

The P:V atomic ratio was checked by chemical analysis. The surface areas were measured according to the BET method, using N_2 at −195°C: 2.0, 10, 0.5, and 0.5 m^2/g were found, respectively, for P_1Va,O_2, P_1Vb,O_2, α-$VOPO_4$(d), and β-$VOPO_4$(e). Little change is expected for other P:V ratios since the greater influence on surface area seems to be due to the possible existence of vanadyl oxalate.

B. Apparatus and Procedure

X-ray diffraction (XRD) diagrams were obtained with CGR Seeman Bohlin chambers, or a diffractometer, using Cu$K\alpha$ radiation. Powdered quartz was added as an internal standard.

Electron diffraction patterns were obobtained with a JEOL 100 C electron microscope.

Infrared spectra of samples dispersed in KBr disks were recorded on a Perkin Elmer 577 spectrophotometer, from 4000 to 250 cm^{-1}.

Diffuse reflectance spectra were recorded on a Beckman DK2A spectrophotometer, from 2600 to 200 nm, using MgO as standard.

DTA was run on a DuPont 990 thermal analyzer, using the 1200°C furnace at 2.5, 5, or 10°C/min rate.

TGA was obtained on a Setaram MTB 10-18 microbalance. Samples in Pt or quartz crucibles were heated in flowing atmospheres of various gases such as N_2, O_2, air, butene, etc. . . (0.5 liter hr^{-1}).

C. Catalytic Activity and Selectivity Measurements

The vapor phase oxidation of 1-butene was carried out using a conventional flow reactor at atmospheric pressure. The stainless steel reactor (200-mm length, ϕ = 25 mm), containing 30 ml of supported catalyst (or broken pieces), was immersed in a

[1] $P_{0.5}Va,O_2$: catalyst P:V = 0.5:1 prepared by method (a), calcined under O_2.

TABLE 2

Identification of P:V Catalysts

Catalysts	Before reaction	After catalytic reaction
$P_{0.5}Va\ O_2$	β-$VOPO_4 + V_2O_5$	$(VO)_2P_2O_7$
$P_1Va\ O_2$	β-$VOPO_4$	$(CO)_2P_2O_7$
$P_1Vb\ N_2$	$(VO)_2P_2O_7$	$(VO)_2P_2O_7$[+ β-$VOPO_4$]^a
$P_1Vc\ O_2$	α-$VOPO_4$	$(VO)_2P_2O_7$
$P_{1.2}Va\ O_2$	β-$VOPO_4$	$(VO)_2P_2O_7$[+β-$VOPO_4$]
$P_{1.6}Va\ O_2$	$VO(PO_3)_2$	$(VO)PO_3)_2$[+ $VO)_2P_2O_7$]
$P_{1.6}Vb\ N_2$	$V(PO_3)_3$	$V(PO_3)_3 + VO(PO_3)_2$
$P_{1.8}Va\ O_2$	$VO(PO_3)_2$	$VO(PO_3)_2 + (VO)_2P_2O_7$
$P_{2.0}Va\ O_2$	$VO(PO_3)_2$	$V(PO_3)_3 + VO(PO_3)_2$

^{a} The compounds in square brackets are sometimes found to be mixed with the first phase indicated.

SiO_2 fluidized bed, heated, and regulated at the required temperature.

The concentration of the feed was 1 vol% of 1-butene in air. The reaction temperature varied from 300 to 450°C and the flow rate from 50 to 150 liter hr^{-1}. The contact time was defined as catalyst volume (30 ml) per total flow rate (ml s^{-1}) and varied from 0.7 to 1.8 sec. Feeding gases were preheated (115°C) and exit gases were heated to 115°C to prevent MAA condensation. Their composition was analyzed by gas chromatography. The main part of the effluent leaving the reactor passed through water bubblers (5°C), then was directed to two chromatographs for analysis of permanent gases (O_2, N_2, CO, CO_2) and hydrocarbons. The other part of the effluent, taken before the water bubblers, was analyzed for oxidized compounds (aldehydes, ketones, acids, furan, and MAA).

III. RESULTS

1. *Influence of Preparation on the Oxidation State of Vanadium Atoms*

Qualitatively, the oxidation state of vanadium in the V–P–O catalysts depends on three factors: (i) the nature of the precursors, (ii) the gaseous atmosphere during the calcination, (iii) the phosphorus content.

If ammoniated precursors (e.g., NH_4VO_3) are used, ammonia will diffuse through each grain of the catalyst during the calcination, and then will reduce V^{5+} to V^{4+} (P:V = 1:1), or to V^{4+} and V^{3+} (P:V > 1:1): Consequently nitrogen atmosphere will enhance the reduction of V^{5+}, while oxygen will oxidize V^{4+} and/or V^{3+}, to a greater or lesser extent (Table 2).

When the phosphorus content increases, it is more and more difficult to keep the vanadium atoms in their higher oxidation state, and oxygen will be necessary to obtain $VO(PO_3)_2$ by calcination instead of $V(PO_3)_3$.

2. *Structural Properties of the Catalysts*

The catalysts have been characterized mainly by XRD, infrared and ultraviolet visible spectroscopies, before and after the catalytic reaction. As shown in Table 2, they are generally composed of β-$VOPO_4$ and $(VO)_2P_2O_7$. In the samples P:V > 1.6:1 the phases $VO(PO_3)_2$ and $V(PO_3)_3$ are present. Since we attempt in this work to elucidate how the properties of the catalysts are related to those of the constituent phases, a review of these structures was necessary.

(*a*) *Crystalline structures.* Pure $VOPO_4$ crystallizes in two forms, α and β, respectively, isostructural with α- and β-$VOSO_4$. XRD patterns were indexed in tetragonal and orthorhombic systems, as indicated in Table 3 (*19–21*). On account of the dissym-

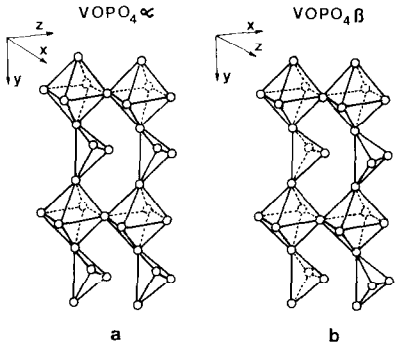

FIG. 1. Crystalline structures of $VOPO_4$; linking between VO_6 octahedra and PO_4 tetrahedra (schematic drawings): (a) in α-$VOPO_4$; (b) in β-$VOPO_4$.

TABLE 3

X-Ray Patterns of Pure V–P–O Phases[a]

β-$VOPO_4$			α-$VOPO_4$[b]			$(VO)_2P_2O_7$			$VO(PO_3)_2$		
d(Å)	I/I_0	hkl	d(Å)	I/I_0	khl	d(Å)	I/I_0	hkl	d(Å)	I/I_0	hkl
5.19	s	101	4.37	w	110	6.28	w	102	3.97	s	011
4.60	s	011	4.11	w	001	5.65	w	111	3.88	s	220
3.96	w	111	3.100	s	200	4.79	w	200	3.47	w	130
3.89	w	200	3.000	m	111	4.08	vw	113	3.217	m	211
3.48	m	002	2.193	w	220	3.87	vs	020	2.777	vw	301
3.40	vs	201	1.960	s	310	3.137	vs	204	2.738	vw	040
3.18	m	102	1.550	s	400	2.982	m	302	2.471	s	321
3.068	vs	020	1.517	m	222	2.906	w	115	2.452	w	420
2.974	m	212	1.461	w	330	2.655	m	106	2.254	vw	141
2.640	m	121				2.435	m	224	2.034	m	112
2.410	w	220				2.399	w	400	1.981	vw	202
2.209	m	122				2.362	w	322	1.947	m	051
2.172	m	013				2.271	w	133	1.941	m	431
2.093	vw	113				2.204	w	117	1.937	m	440
1.993	w	203				2.083	m	306	1.832	vw	251
1.961	m	031				1.981	w	127	1.804	vw	610
1.947	w	400				1.934	w	040	1.786	vw	441
1.701	w	104				1.840	w	326	1.730	vw	260
1.638	w	114				1.826	vw	424	1.673	vw	042
1.608	w	223				1.644	vw	244	1.632	vw	332
1.539	s	214				1.633	w	1010	1.583	vw	451
1.534	s	033				1.567	m	506	1.580	w	541
		040				1.492	vw	604	1.519	w	460
1.505	s	133				1.417	m	620	1.468	w	071
1.459	vw	332				1.459	m	522	1.406	w	103
1.444	vw	304									
D_{2h}^{16}–P_{nma}			C_{4h}^{3}–$P_{4/n}$			C_{2v}^{2}–P_{nc2_1}					
a = 7.770 Å			a = 6.20 Å			a = 9.751 Å			a = 10.96 Å		
b = 6.143 Å			c = 4.11 Å			b = 7.738 Å			b = 10.95 Å		
c = 6.965 Å						c = 16.568 Å			c = 4.254 Å		
z = 4			z = 2			z = 4			z = 4		
(*20*, *21*)			(*21*)			(*22*, *23*)			(*23*, *25*)		

[a] Lines intensity: vs, very strong; s, strong; m, medium; w, weak; vw, very weak.

[b] Owing to the preparation mode, the pattern and parameters are slightly different from those in Ref. (*19*).

metry of VO_6 pseudo-octahedra, the main feature of both forms of $VOPO_4$ is a layer structure, which allows comparison with ReO_3-type matrices (*21*). Pseudo-octahedra share corners with PO_4 tetrahedra giving ribbons or sheets in the (010)β plane and (001)α plane whose texture is plateletlike (Fig. 1).

$(VO)_2P_2O_7$ was not found to be isostructural with any crystalline compound (*22*). A study of a monocrystal is in progress (*23*) and will be published later. The crystalline pattern is composed of edge-sharing octahedra linked to pyrophosphate tetrahedra in a rather simple distribution; ir and uv-visible spectra, respectively, confirmed the existence of the $P_2O_7^{4-}$ anion and the vanadyl group VO^{2+}.

Electron microscopy and diffraction on $(VO)_2P_2O_7$ samples confirmed the XRD results. However, patterns of spent reduced catalysts revealed additional interesting features as was already the case for V_2O_5 reduction (*26*) (Fig. 2). Frequently the

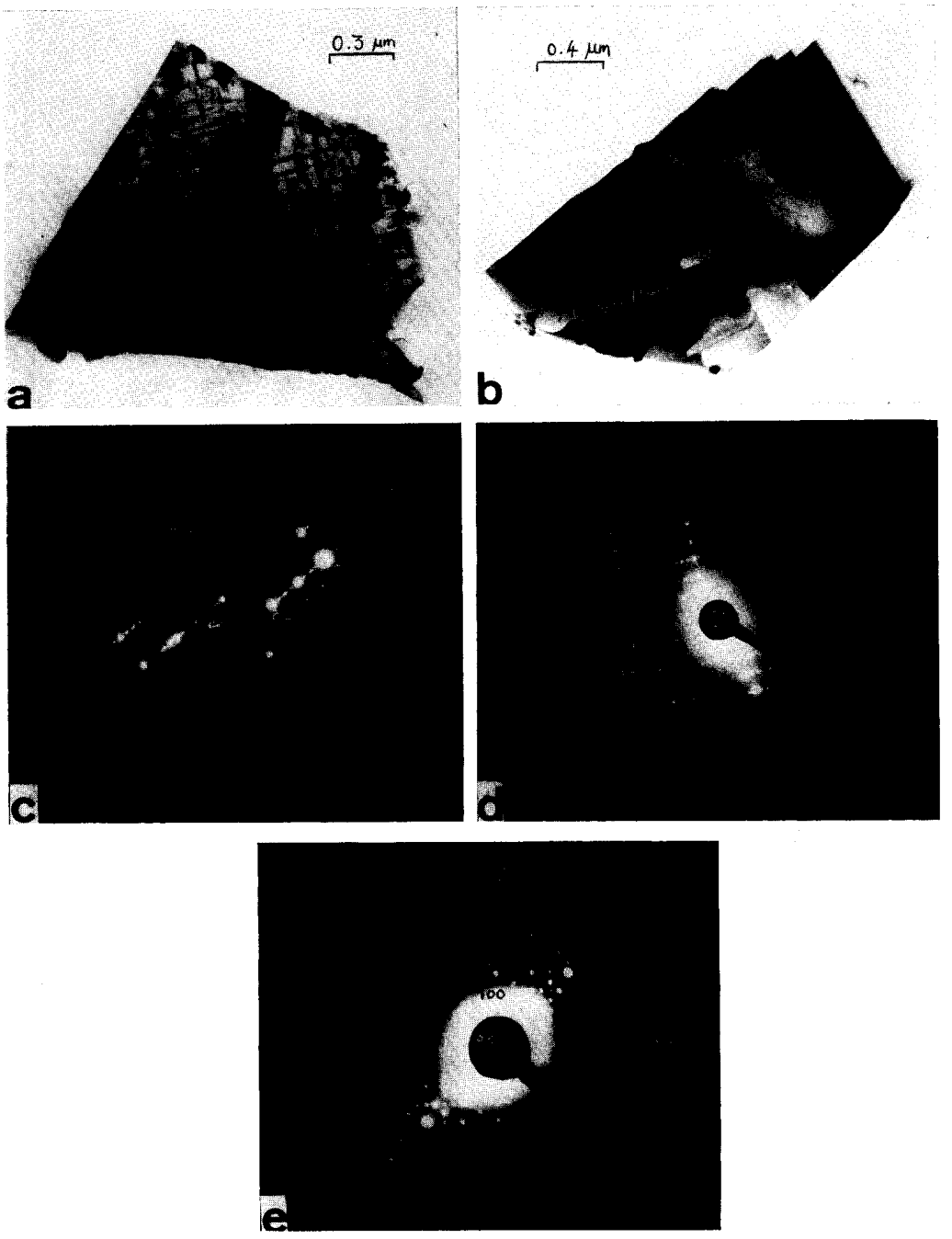

FIG. 2. Electron microscopy and diffraction on spent catalysts P:V = 1:1 [$(VO)_2P_2O_7$]: (a) crosshatch-oriented texture; (b) microdomains and antiphase boundaries; (c) plane (100): streaking along 001; (d) plane (110): streaking along 001; (e) example of supersturcture due to periodicities in 010; plane (010).

texture is crosshatch-oriented; superstructures, microdomains, and antiphase boundaries can be seen. Streaking along g(001) or g(011) is often observed, indicating that disorder occurs in these directions.

The $VO(PO_3)_2$ phase is present in P:V

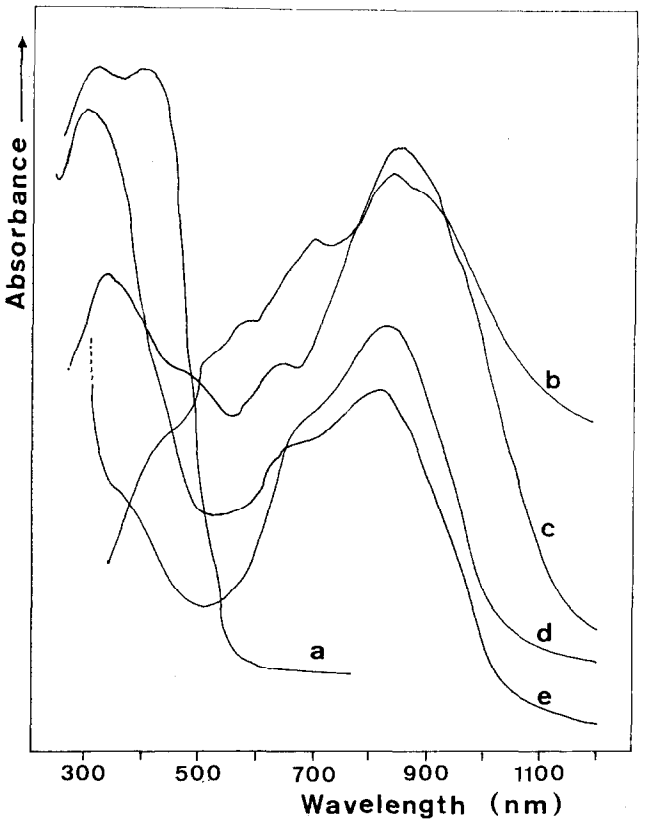

FIG. 3. Diffuse reflectance spectra (1200–200 nm) of $VOMoO_4$ and V–P–O catalysts: (a) P_1VaO_2 (=$VOPO_4$); (b) $VOMoO_4$; (c) spent P_1VaO_2 = $(VO)_2P_2O_7$; (d) $VO(PO_3)_2$; (e) $P_{1.6}Vb$, air.

= 1.6:1 to 2:1 XRD patterns (Tables 2 and 3). The crystalline pattern is composed of infinite chains of metaphosphate anion and $VO(O)_5$ octahedra as confirmed by spectroscopy. The disorder found along the "*c*" axis (*23*, *24*) is probably responsible for the slight differences observed with XRD patterns in the work of Lavrov *et al.* (*25*).

(*b*) *Diffuse reflectance spectroscopy.* As expected from a d^0 transition metal ion, only charge transfer bands occur in $VOPO_4$ samples and catalysts P_1VaO_2 or P_1VbO_2 (Table 4, Fig. 3). On the contrary, $(VO)_2P_2O_7$ and $VO(PO_3)_2$ spectra show four bands in the crystal field range, which are known to be due to *d–d* transitions. Assuming the symmetry of the vanadium environment to be C_{2v}, bands I, II, III are assigned, respectively, to transitions $^2E \rightarrow {}^2B_2$, $^2B_1 \rightarrow {}^2B_2$, and $^2A_1 \rightarrow {}^2B_2$. Band III is often considered as due to charge transfer, or overlapped by it (*27*). Spent catalysts P_1Va and $P_{1.6}Va$ resemble, respectively, $(VO)_2P_2O_7$ and $VO(PO_3)_2$.

(*c*) *Infrared spectroscopy.* The various phosphate anions can be recognized from infrared spectra (Fig. 4); analyses were carried out simply by reference to the site symmetry of the anion in the compound (*28*).

Four fundamental vibrations are known for the PO_4^{3-} anion in T_d symmetry, giving nine vibrations for C_s symmetry occurring in β-$VOPO_4$ (Table 5). Our assignments are in agreement with those reported by Bhargava and Condrate (*29*).

The pyrophosphate anion has been widely studied; although its symmetry is

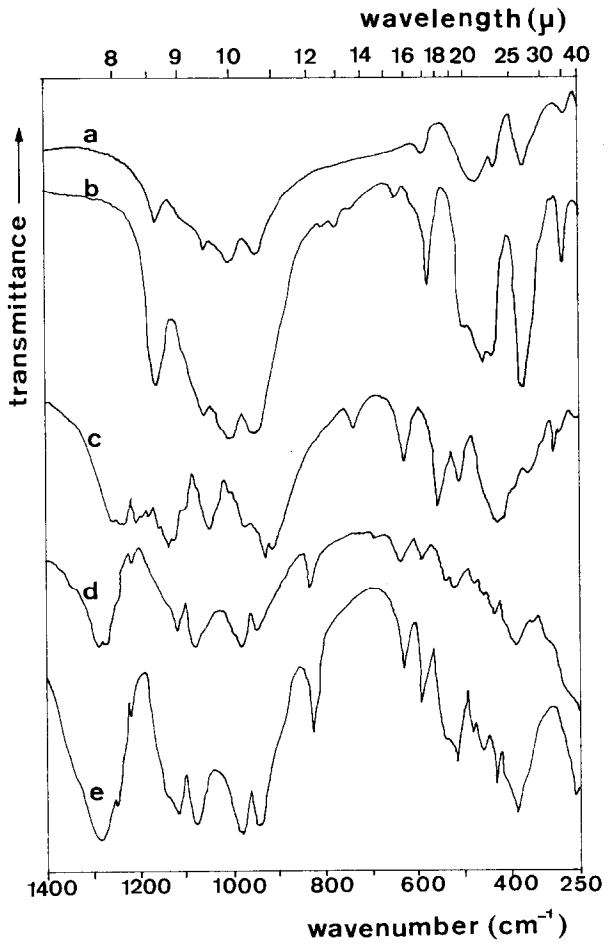

FIG. 4. Infrared spectra of V–P–O compounds (1400–250 cm^{-1}): (a) P_1VaO_2; (b) β-$VOPO_4$; (c) $(VO)_2P_2O_7$; (d) $P_{1.6}Vb$, air; (e) $VO(PO_3)_2$.

often C_{2v}, C_s, or C_1, a D_{3h} approximation has been found accurate enough to describe the spectra of $Me_2^{2+}P_2O_7$ compounds (*30*). Twelve vibrations are infrared active ($3A_1' + 3A_2'' + 3E'' + 3E'$) instead of 21 in C_s symmetry.

Metaphosphate anion spectra in $Me^{2+}(PO_3)_2$ compounds were only qualitatively described. In $VO(PO_3)_2$, as in $P_{1.6}VaO_2$ and $P_{1.8}VaO_2$, the evident splitting lying about 1020 cm^{-1} is due to coupling schemes between P–O and V–O stretching modes.

In all these cases, some uncertainty remains about the actual wavenumber of the V=O stretching mode, on account of the complexity of the spectra. The obtained values of 995 cm^{-1} in β-$VOPO_4$ and 980 cm^{-1} in $(VO)_2P_2O_7$ may be tentatively assigned to this mode, which is known to occur between 1030 cm^{-1} (V_2O_5, $VOCl_3$) and 950 cm^{-1} (inorganic vanadyl complexes) (*31*).

3. *Kinetic and Thermodynamic Experiments*

(a) The decomposition of precursors and of $(NH_4)_2[(VO)_2C_2O_4(HPO_4)_2]\cdot 5H_2O$ studied by DTA have been described in earlier papers (*15*, *21*).

The DTA reduction of a P_1VaO_2 (β-

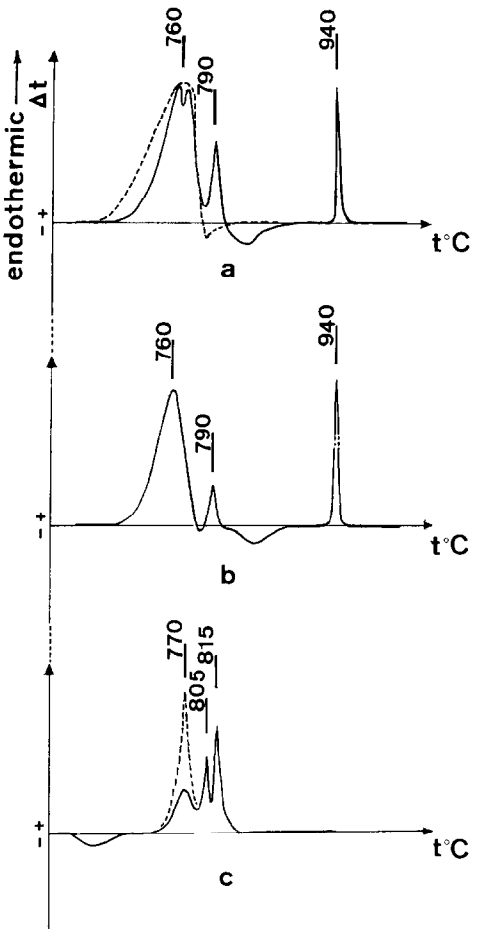

FIG. 5. DTA reduction and reoxidation of P:V = 1:1 compounds (heating rate: dashed line 2.5°C/min; full line 10°C/min): (a) reduction of α-$VOPO_4$; (b) reduction of β-$VOPO_4$; (c) reoxidation of $(VO)_2P_2O_7$.

$VOPO_4$) catalyst or of α-$VOPO_4$ under flowing nitrogen is dependent on the heating rate (Fig. 5a and b). Endothermic peaks about 780°C account for this reduction, and are followed by the crystallization (exothermic) and melting (940°C) of $(VO)_2P_2O_7$. The transformation at 790°C is inhibited if the heating rate is kept at 2.5°C/min: Under these conditions, a metastable VPO_x compound is assumed to form ($4.72 < x < 4.76$). The reoxidation of $(VO)_2P_2O_7$ (Fig. 6c) under oxygen at 770°C is complete at 790°C, yielding

TABLE 4

Diffuse Reflectance Spectra of [V–P–O] Phases and $VOMoO_4$[a]

ν cm^{-1}	I	II	III	Charge transfer	
$VOPO_4$ α, β				23,900	31,700
$VOMoO_4$	11,760	17,240	19,090	27,030	
	14,290				
$(VO)_2P_2O_7$	11,760	15,600	21,280		33,300
	13,400				
$VO(PO_3)_2$	12,050	14,700		25,600	33,400
P/V = 1.6 catalyst	11,500				
	12,340			25,000	29,400
	14,290				

[a] $VOMoO_4$ is taken as an example of VO^{2+}-containing oxysalts.

β-$VOPO_4$ which melts at 815°C after a vitreous transition (805°C) (*21*).

(b) Cycles of isothermal TGA redox

TABLE 5

Wavenumbers and Vibration Assignments in β-$VOPO_4$ and $(VO)_2P_2O_7$ Infrared Spectra

β-$VOPO_4$				
T_d	$\bar{\nu}$ cm^{-1}	C_s	$\bar{\nu}$ cm^{-1}	Modes
			1155	
			1060	
ν_3 (T_2)	1017	$2A' + A''$	1045	ν_{as}P–O stretch
			995	V=O stretch
ν_1 (A_1)	938	A'	940	ν_s P–O stretch
			640	
			600	
ν_4 (T_2)	567	$2A' + A''$	580	δ_{as}O–P–O
			480	
ν_2 (E)	420	$A' + A''$	430	δ_sO–P–O
			360	

$(VO)_2P_2O_7$				
D_{2h}	$\bar{\nu}_{calc}$	C_s	$\bar{\nu}$ cm^{-1}	Modes
			1265	
A'_1	1212	A'	1250	
			1215	ν_{as} PO_3
			1185	
A''_2	1165	A'	1160	
			1145	
E'	1124	$A' + A''$	1125	
E''	999	$A' + A''$	1055	
			1010	ν_s PO_3
			980	V=O stretch
A''_2	940	A'	935	
A'_1	909	A'	920	ν_{as} P–O–P
E'	707	$A' + A''$	740	ν_s P–O–P
E''	615	$A' + A''$	635	
A''_2	553	A'	555	δ_{as} PO_3
A'_1	477	A'	515	
			460	δ_s PO_3
E''	432	$A' + A''$	430	
			400	

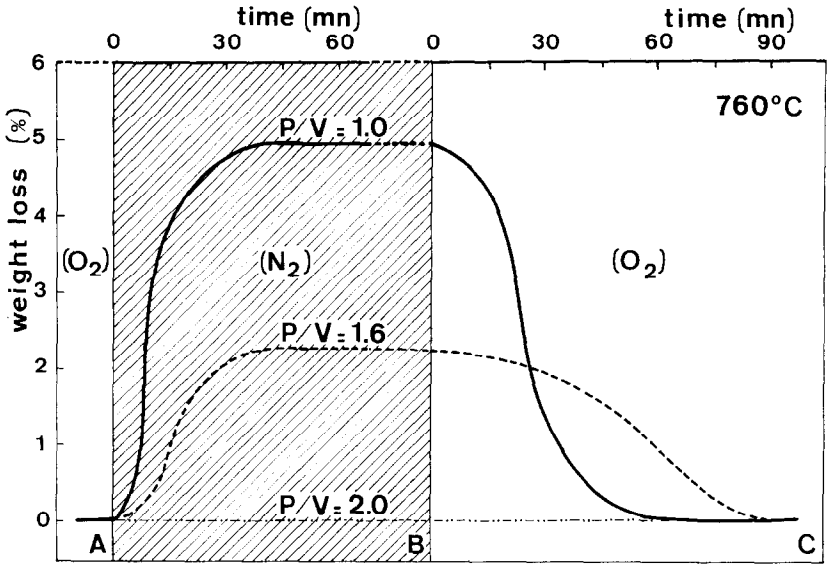

FIG. 6. Thermograms of isothermal redox cycles for P_1VaO_2, $P_{1.6}VaO_2$, and P_2VaO_2 at 760°C in gaseous atmosphere: oxygen in (A) and (C), nitrogen in (B).

were performed at 760°C to compare the behavior of P_1VaO_2, $P_{1.6}VaO_2$, and P_2VaO_2. The catalysts were heated to 760°C in oxygen atmosphere, until no more weight variation could be detected (Fig. 6A); then N_2 was allowed to flow in the apparatus. The reduction being complete (Fig. 6B), O_2 was admitted again (Fig. 6C), and this cycle was repeated several times. XRD patterns obtained on samples quenched in Fig. 6A, B, and C reveal β-$VOPO_4$ (A), $(VO)_2P_2O_7$ (B), and β-$VOPO_4$ (C) for P_1VaO_2, and $VO(PO_3)_2$ in each case for P_2VaO_2. The situation appears more complex for $P_{1.6}VaO_2$: in A, XRD pattern of $VO(PO_3)_2$; in B, a mixture of $(VO)_2P_2O_7$ and $VO(PO_3)_2$; and in C, a mixture of β-$VOPO_4$ and $VO(PO_3)_2$. Several changes in temperature reveal the presence of a divariant equilibrium for P_2VaO_2 samples.

(c) Since $VOPO_4$ and $(VO)_2P_2O_7$ are the components of the redox system in the catalysts, microgravimetric equilibrium measurements between these pure phases have been carried out under controlled pO_2 (Fig. 7). The reduction of α-$VOPO_4$ occurring at 760°C and $pO_2 = 10^{-5}$ atm ("Air Liquide" U-grade nitrogen gas), the so-called "direct control" using synthetic mixtures of oxygen and nitrogen can be used. Moreover, the rate of transport of O_2 to or from the sample in the temperature range is fast enough for the equilibrium to be reached in a measurable time (*22*).

According to the temperature, the isotherms delimit different redox reactions:

$t<750$°C
$$VPO_5 \rightleftarrows VPO_{4.5} + 0.25\,O_2 \quad (1)$$

$t>750$°C
$$VPO_5 \rightleftarrows VPO_{4.75} + 0.125\,O_2 \quad (2)$$
$$VPO_{4.75} \rightleftarrows VPO_{4.5} + 0.125\,O_2 \quad (3)$$

From Fig. 7, it can be seen that the reduction of α-$VOPO_4$ leads to the formation of homogeneity ranges, as well as reoxidation of $(VO)_2P_2O_7$ ex α-$VOPO_4$. Moreover, the reoxidation of $(VO)_2P_2O_7$ takes place at a pO_2 different from that obtained when $VOPO_4$ is reduced. The study of this hysteresis is still in progress.

(d) Reductions of $VOPO_4$(e) and V_2O_5 by hydrogen and 1-butene have been performed, followed by reoxidation in O_2 or air. In either case, the reduction proceeds

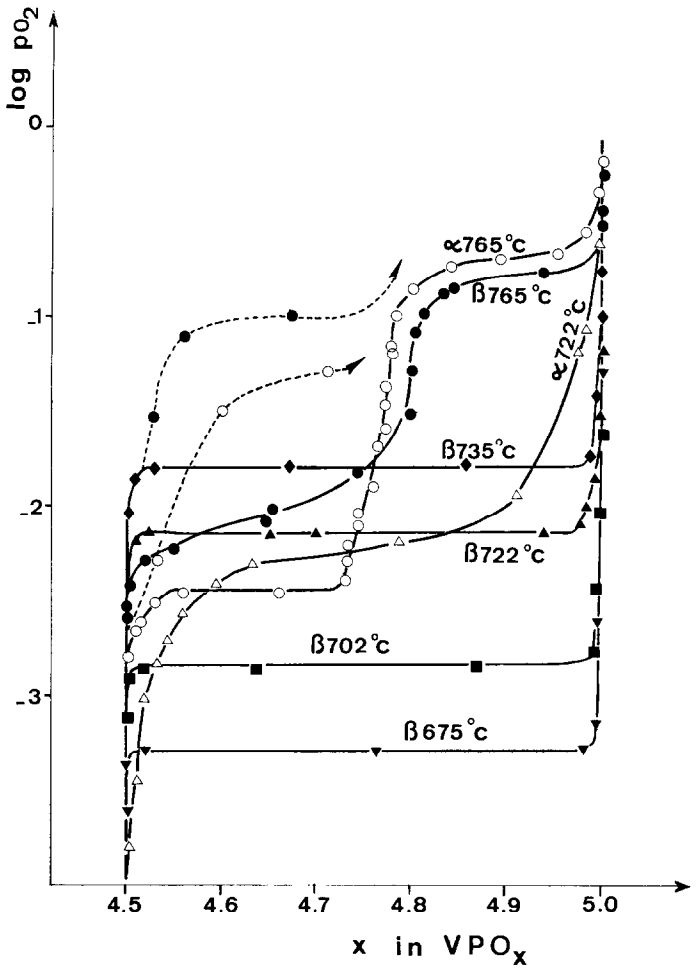

FIG. 7. Oxygen equilibrium pressure above $VOPO_4$–$(VO)_2P_2O_7$ system at various temperatures; open symbols: reduction of α-$VOPO_4$; full symbols: reduction of β-$VOPO_4$. Dashed line: reoxidation of $(VO)_2P_2O_7$ at 765°C (hysteresis).

faster than the reoxidation (Fig. 8), and the rate is controlled by diffusion in micro TGA conditions. Although V^{3+} ions are produced during the reduction, the final $VPO_{4.5}$ stoichiometry (wt% loss 4.95) can be kept under 1-butene, contrary to the reduction of V_2O_5 which proceeds slowly to V_2O_3.

(e) The reduction of a P_1VaO_2 sample under catalytic conditions has been carried out in the microbalance (Fig. 9). P_1VaO_2 was first heated under O_2 to 700°C to be sure of the V^{5+} amount ($VOPO_4$), then the temperature was decreased to 420°C and air-butene was allowed to flow in the apparatus: The steady state was reached about 7 hr later, the composition of the discharged solid being about $VPO_{4.74}$. The resulting sample was reduced under N_2 at 750°C ($VPO_{4.5}$), and air–butene was admitted again at 420°C: The reoxidation proceeded faster, the final composition being in this case $VPO_{4.65}$.

4. *Catalytic Activity and Selectivity Measurements*

Here the main purpose was to compare the catalytic properties of the V–P–O cata-

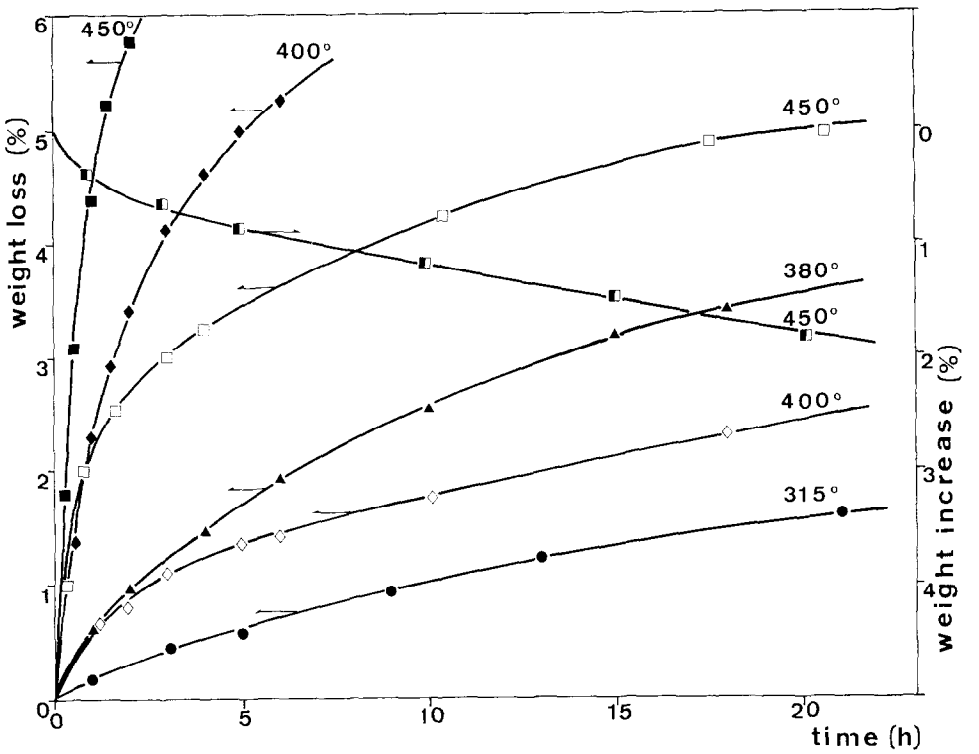

FIG. 8. Kinetics of reduction of β-$VOPO_4$ by H_2 (full symbols) and 1-butene (open symbols), as a function of the composition of the solid x in VPO_x. Reoxidation under O_2: half-full squares.

lysts prepared in the present work with those reported in the literature (*14*, *32*).

The reaction butene → MAA has been widely studied (*33–35*). The butene transformation proceeds by consecutive steps:

$$\left.\begin{matrix}\text{1-butene}\\ \Updownarrow\\ \text{2-butenes}\end{matrix}\right\} \rightarrow \text{butadiene} \rightarrow \text{furan} \rightarrow$$

$$\text{MAA} \rightarrow \text{CO, CO}_2,$$

and has already been interpreted by a "rake" scheme (*36*, *37*). Numerous side products are formed in parallel reactions and revealed by chromatographic analysis (acetaldehyde, acrolein, methacrolein, acetic, propionic, and acrylic acids, and in smaller amounts, methyl ethyl ketone, methyl vinyl ketone and crotonaldehyde).

The catalytic properties of samples calcined in air were found to be the most interesting, probably because some V^{4+} sites are already present. The activity and selectivity of P_1Vb,air were found to be better than those of P_1Va,air or those described in the literature (*32–34*). The activity of supported P_1Vb,air (α-$VOPO_4$/Al_2O_3) decreases rapidly with time, although activity and selectivity of P_1VcO_2 (α-$VOPO_4$, too) are very close to those of P_1VaO_2. The catalyst P_2Va,air is not active.

The conversion of 1-butene to the main products (mole%) on P_1Vb,air and selectivity to MAA are plotted against the reactor temperature in Fig. 10: 53 mole% of MAA could be obtained around 400°C. Figure 11 represents the yields in butadiene, furan, and MAA for P_1Vb air, $P_{1.6}Vb$ air and for V_2O_5 prepared as in Ref. (*14*); selectivity curves for MAA production account for the different behaviors of catalysts V–O and V–P–O. The selectivities in MAA against P:V stoichi-

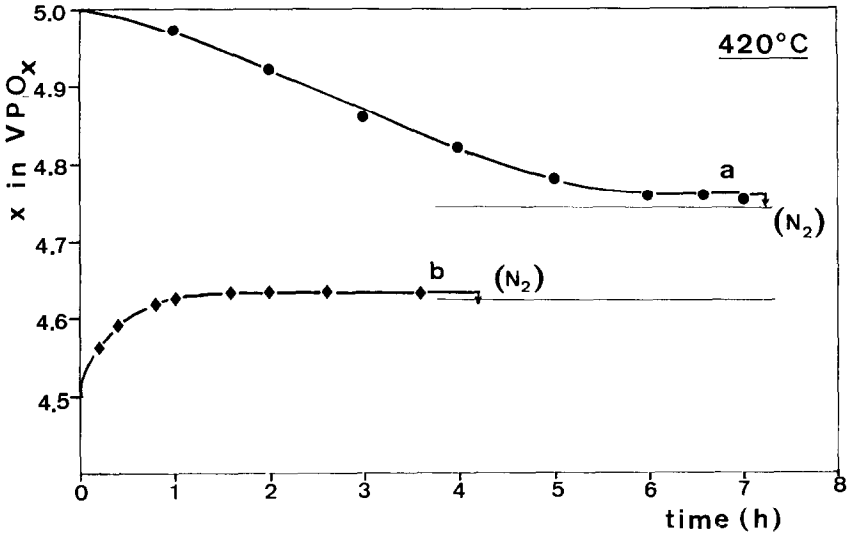

FIG. 9. Achievement of the steady state at 420°C (1-butene in air: 1%) for P_1VaO_2 catalyst: (a) reduction of P_1VaO_2; (b) reoxidation of reduced P_1VaO_2.

ometry reach a limiting value between P:V = 1:1 and 1.8:1 and fall when P:V = 2:1 (Fig. 12).

IV. DISCUSSION

These experiments first show that, for an increasing P:V atomic ratio between 0.5:1 and 1:1 where $VOPO_4$ and $(VO)_2P_2O_7$ are present, the V–P–O catalysts become more and more selective. In the range $1:1 < P:V < 1.8:1$ the selectivity reaches an optimal and approximately constant value (Fig. 12). Since both $VOPO_4$ and $(VO)_2P_2O_7$ are present (Table 2 and Fig. 6) the same redox process takes place in this range, besides $VO(PO_3)_2$. Out of these limits, i.e., for $P:V < 0.5:1$ and P:V = 2:1, either V_2O_5 or $VO(PO_3)_2$ (which cannot be reoxidized) are found and the selectivity decreases.

Since no compound other than $VO(PO_3)_2$ could be discerned in the XRD pattern of P:V = 1.6:1 catalysts, the question arises whether the catalyst is composed of $VO(PO_3)_2$ mixed with an amorphous phase (containing V^{5+}) or of a solid solution such as $VO\,[(PO_3)_x(VO_3)_{1-x}]_2$. The existence of such a homogeneity range ($x = 0.92$ for P:V = 1.6:1) should be justified by the disorder found along the "*c*" axis. The rate of substitution was too weak to observe a significant shift of the XRD lines, and only change of their intensity was detected.

From these results, and according to our earlier observations (*22*), a first conclusion can be drawn, namely, that a substantial selectivity is obtained only when $VOPO_4$ and $(VO)_2P_2O_7$ phases are present. Consequently, it is convenient to relate the selectivity of V–P–O catalysts to the most essential and interdependent properties of these two phases.

Macroscopic Properties

1. Kinetic and structural results show that, in the steady state, $(VO)_2P_2O_7$ is the predominant form (Fig. 9 and Table 2), and in the absence of air, 1-butene is oxidized at 450°C (Fig. 8), as observed also in the case of V_2O_5. Thus, not only surface but also bulk oxygen atoms are concerned in a classic Mars and Van Krevelen mechanism (*39*), in which reduction of $VOPO_4$ is faster than $(VO)_2P_2O_7$ reoxidation, as long as the steady state is not definitely reached.

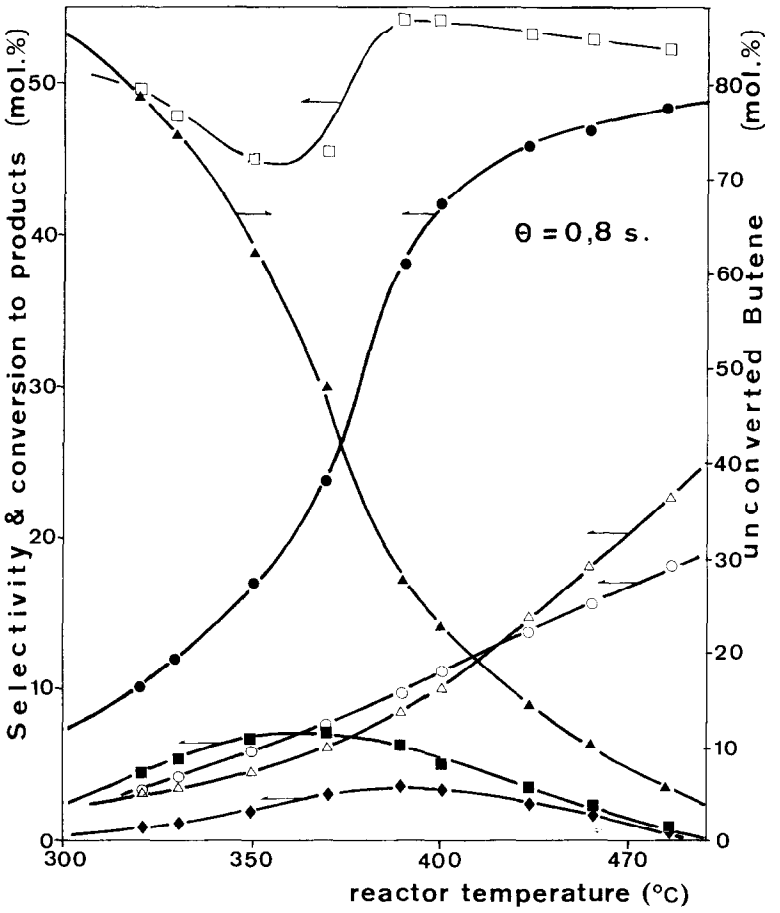

FIG. 10. Unconverted butene (▲), yields in main products and selectivity in MAA vs temperature of the reaction. Yields in: ●, MAA; ■, butadiene; ◆, furan; ○, CO_2; △, CO; □, selectivity in MAA.

2. The structural features of the solid phases in the V–P–O system are similar to those observed in V_2O_5 and its suboxides in spite of the existence of tetrahedral PO_4 and P_2O_7 units. Their layer structure results from the alternation of short covalent (σ, π) and long (σ) vanadium–oxygen bonds in a direction perpendicular to the natural cleavage plane; the low symmetry of the vanadium environment (C_s) is then expected to be unchanged at the surface.

3. The latter property, common to V_2O_5 and other ReO_3-type crystals, explains why the so-called R″ mechanism of isotopic exchange of oxygen is exhibited by V_2O_5 (*40*). The single energy state of oxygen detected by isochore experiments (*41*), i.e., the identity between the heat of adsorption of oxygen and the enthalpy of reduction to suboxide ($\Delta H_{298°} = 60$ kcal/mole O_2) is another fact that allows us to use, in this special case, bulk thermodynamic data in order to characterize the active oxygen (*38*).

The approximate change of standard enthalpy of the redox system can be obtained from equilibrium measurements of pO_2 over the system, by means of empirical formulas established for oxide redox processes (*42*): $\Delta H_{298°}(O_2) = 52$ kcal/mole O_2. Conversely, the change of standard free energy at 400°C is $\Delta G_{673°}(O_2) = 23$ kcal/mole O_2. $\Delta H_{298°}(O_2)$ is considered as an

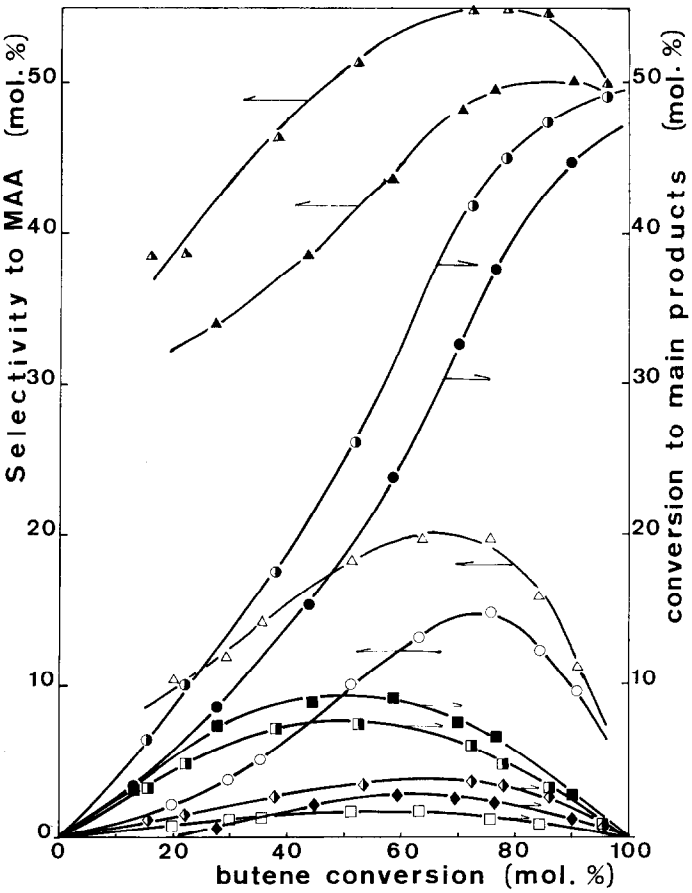

FIG. 11. Conversion to butadiene, furan, and MAA and selectivity in MAA for P_1Vb, air, $P_{1.6}Vb$, air, and V_2O_5 catalysts (half-full, full, and open symbols, respectively). Squares, butadiene; diamonds, furan; circles, conversion to MAA; triangles, selectivity to MAA.

internal energy, and has generally been related to catalytic activity. The available redox energy is measured by $\Delta G_{T^\circ}(O_2)$, being also the chemical potential μO_2 of the lattice oxygen involved in the catalytic process at a given temperature. ΔH and ΔG are intrinsic bulk properties of the V–P–O catalysts which should be used for any correlation.

However, for the majority of oxide catalysts, the first layers are only concerned in the catalytic process, and the active redox process takes place without any noticeable modification of the crystalline structure. In such cases, the integral bulk free energy $\Delta G^\circ(O_2)$ must be replaced by the partial molar quantity $\Delta g^\circ(O_2)$ relative to homogeneous oxygen; these values can be deduced directly from isochore experiments (generally used for ΔH_{298° evaluation), but then depend not only on T, but also on θ (fractional coverage) (*41*) or x (degree of reduction) (*43*).

4. Concerning the acid–base properties of V–P–O catalysts, it has been shown (*10*) that an addition of P_2O_5 to V_2O_5 causes a sharp decrease in both surface area and acidity (P:V > 0.5:1), and correlatively an increase in selectivity. Further addition of P_2O_5 induces no more change in the nature of active species, and consequently, the selectivity reaches a limiting value. These results can be well interpreted by the formation of one phase, $VOPO_4$, from

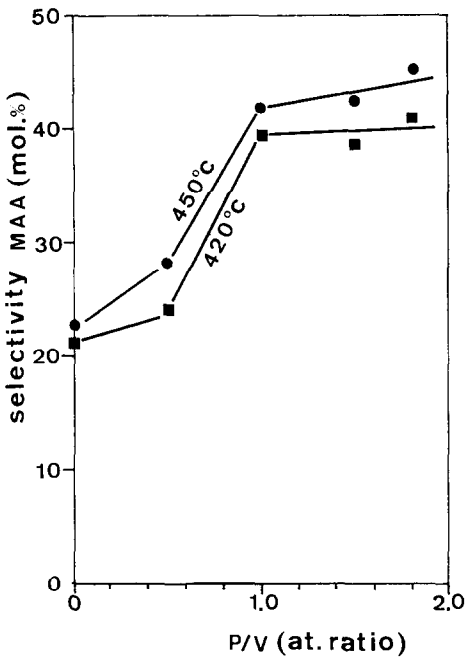

FIG. 12. Selectivity in MAA as a function of vanadium–phosphorus content (P:V atomic ratio).

P:V = 0.5:1 to 1.8:1 as previously shown. Therefore, the surface properties of the catalyst, and then its selectivity, cannot be considered as a simple, continuous, and additive function of the increasing P_2O_5 content. On the contrary, they exhibit discrete and sharp variations for the composition where a thermodynamic phase appears, and remain approximately constant until inactive $VO(PO_3)_2$ replaces $VOPO_4$.

The same interpretation may be given for other binary catalysts, since experimental correlations between selectivity and composition generally exhibit a maximum, precisely for a composition corresponding to the formation of a phase. In addition to the example of USb_3O_{10}, which has been claimed to be responsible for activity and selectivity in ammoxidation of propylene (*44*), the best conversion to MAA from benzene is found for 33% MoO_3 in V_2O_5 (*45*), known as the Kihlborg phase (*46*). In propylene conversion to acrolein on SnO_2–Sb_2O_5 (*47*) the selectivity increases continuously up to 15% Sb_2O_5, i.e., in the range of formation of a solid solution, which again is a thermodynamic phase. Above this composition, the solid solution coexists with free Sb_2O_5 and the selectivity increases no longer.

Microscopic Properties

The disorderly reflections observed by electronic diffraction on spent catalysts P:V = 1:1 (Fig. 2) indicate that, in steady state conditions, microdomains of $VOPO_4$ still coexist within larger domains of $(VO)_2P_2O_7$. The boundaries between these microdomains are thought to be coherent because the two structures fit closely: for example, the lattice misfit computed between $(20\bar{3})$ $VOPO_4$ and (102) $(VO)_2P_2O_7$ planes is only 2–4%. This kind of interfacial relationship has already been observed between V_2O_5 and V_6O_{13} or VO_2(B) (*48*).

Moreover, the hysteresis phenomena that we observed in microgravimetric and kinetic experiments (Figs. 7 and 9), have been interpreted by the formation of microdomains termed "hybrid crystals," first in the case of crystalline allotropy (*49*) and later in the thermal reduction of V_2O_5 (*50*). The same situation arises for *unsupported* catalysts P:V = 1:1 in steady state conditions: Consequently, the atoms located near the interface boundaries are in long-lived excited states and are assumed to play the role of active and selective sites. Moreover, whereas in a pure reduction (or oxidation) process the strain produced at the boundaries is compensated mainly by mechanical relaxation (dislocations, etc), the lattice of the catalyst prefers to release a part of its excess energy toward the reactant; it recovers it when reoxidation occurs. As a result, the redox alternation statistically keeps the lattice under strain.

In the case of *supported* catalysts where the selectivity was shown to be dependent of the nature of the active support, the same explanation applies: For example, the electronic interactions between V_2O_5 and

TiO_2 (anatase) are thought to be enhanced by a close crystallographic fit at the interface of the two oxides (*48*).

ACKNOWLEDGMENTS

We are grateful for financial and material support from Rhône-Poulenc Industries. We thank Messrs. Jouy and Van den Bussche (R.P.I.) for valuable discussions; we are also indebted to Dr. Véjux for his creative suggestions and for help in the preparation of the manuscript.

REFERENCES

1. Stone, F. S., *J. Solid State Chem.* **12**, 271 (1975).
2. Hucknall, D. J., "Selective Oxidation of Hydrocarbons." Academic Press, London, 1974.
3. Sachtler, W. M. H., and De Boer, N. H., *in* "Proceedings, 3rd Int. Congr. Catal., Amsterdam 1964," p. 252. North-Holland, Amsterdam, 1965.
4. Moro-Oka, Y., Morikawa, Y., and Ozaki, A., *J. Catal.* **7**, 23 (1967).
5. Simons, T. G. J., Verheijen, E. J. M., Batist, P. A., and Schuit, G. C. A., *Advan. in Chemistry Series* **76**, No. 2, 261 (1968).
6. Shvets, V. A., and Kazanski, V. B., *J. Catal.* **25**, 123 (1972).
7. Krylov, O. V., Pariiskii, G. B., and Spiridonov, K. N. J., *J. Catal.* **23**, 301 (1971).
8. Boreskov, G. K., Venyaminov, S. A., Dzisko, V. A., Tarasova, D. V., Dindoin, V. M., Sazonova, N. N., Olenkova, I. P., and Kefeli, L. M., *Kinet. Katal.* **10**, 1350 (1969).
9. Haber, J., and Grzybowska, B., *J. Catal.* **28**, 489 (1973).
10. Ai, M., and Suzuki, S., *Bull. Chem. Soc. Japan* **47**, 3074 (1974).
11. Haber, J., *Int. Chem. Eng.* **15**, 21 (1975).
12. Cimino, A., *Chim. Ind. (Milan)* **56**, 27 (1974).
13. Pepe, F., and Stone, F. S., *in* "Proceedings, 5th Int. Congress on Catalysis, Florida, 1972," p. 137. North-Holland, Amsterdam, 1973.
14. Ai, M., *Bull. Chem. Soc. Japan* **43**, 3490 (1970).
15. Pulvin, S., Ronis, M., and Courtine, P., *C.R. Acad. Sci. Paris, Ser. C.* **293**, 585 (1976).
16. Preuss, F., and Schug, M., *Z. Naturforsch.* **30b**, 334 (1975).
17. Ladwig, G., *Z. Anorg. Allgem. Chem.* **51**, 2621 (1973).
18. Pulvin, S., and Courtine, P., in preparation.
19. Jordan, B., and Calvo, C., *Canad. J. Chem.* **51**, 2621 (1973).
20. Gopal, R., and Calvo, C., *J. Solid State Chem.* **5**, 432 (1972).
21. Bordes, E., Courtine, P., and Pannetier, G., *Ann. Chim.* **8**, 105 (1973).
22. Bordes, E., and Courtine, P., Réunions Annuelles Soc. Chim. Fr., Marseille 1973 E. Bordes, Thèse, Paris, 1973.
23. Middlemiss, N., and Calvo, C., private communication.
24. Tofield, B. C., and Crane, G. R., *J. Chem. Soc., Dalton Trans.*, 1806 (1975).
25. Lavrov, A. V., Guzeeva, L. S., and Fedorov, P. M., *Inorg. Mat.* **10**, 1869 (1974).
26. Tilley, R. J. D., and Hyde, B. G., *J. Phys. Chem. Solids* **31**, 1613 (1970).
27. Lever, A. B. P., "Inorganic Electronic Spectroscopy." Elsevier, Amsterdam/New York, 1968.
28. Hezel, A., and Ross, S. D., *Spectrochim. Acta* **22**, 1949 (1966).
29. Bhargava, R. N., and Condrate, R. A., *Appl. Spectrosc.* **31**, 230 (1977).
30. Hezel, A., and Ross, S. D., *Spectrochim. Acta* **24A**, 131 (1968).
31. Selbin, J., *Chem. Rev.* **65**, 153 (1965).
32. Seeboth, H., Kubias, B., Wolf, H., and Lücke, B., *Chem. Technol.* **28**, 730 (1976).
33. Ai, M., Boutry, P., and Montarnal, R., *Bull. Soc. Chim. Fr.*, 2775, 2783 (1970).
34. Akimova, L. S., Serebryakov, B. R., and Kolchin, I. K., *Neftekh.* **11**, 545 (1971).
35. Ostroushko, V. I., Kernos, Y. D., and Ioffe, I. I., *Neftekh.* **12**, 362 (1972).
36. Boutry, P., and Montarnal, R., *C.R. Acad. Sci. Paris, Ser. C.* **263**, 1102 (1966).
37. Germain, J. E., and Peuch, J. C., *Bull. Soc. Chim. Fr.*, 1844 (1969).
38. Germain, J. E., *J. Chim. Phys.* **70**, 1048 (1973).
39. Mars, P., and Van Krevelen, D. W., *Chem. Eng. Sci.* **3**, 41 (1954).
40. Novakova, J., *Catal. Rev.* **4**, 77 (1970).
41. Joly, J. P., *J. Chim. Phys.* **72**, 1019 (1975).
42. Kubaschewski, O., *Bull. Soc. Chim. Fr.* **1965**, 1170.
43. Sachtler, W. M. H., Dorgelo, G. J. H., Fahrenfort, J., and Voorhoeve, R. J. H., "Proceedings, 4th Int. Congress on Catalysis, Moscow, 1968," Vol. I, p. 454. Akademiai Kiado, Budapest, 1971.
44. Grasselli, R. K., and Suresh, D. D., *J. Catal.* **25**, 273 (1972).
45. Pyatniskii, Y. I., Ilchenko, N. I., and Golodets, G. I., *Katal. y Katal.* **7**, 5 (1971).
46. Eick, H. A., and Kihlborg, L., *Acta Chem. Scand.* **20**, 1968 (1966).
47. Wakabayashi, G. W., Kamiya, Y., and Ohta, N., *Bull. Chem. Soc. Japan* **40**, 2172 (1967).
48. Véjux, A., and Courtine, P., *J. Solid State Chem.* **23**, 93 (1978).
49. Ubbelohde, A. R., *J. Chim. Phys.* **62**, 33 (1966).
50. Anderson, J. S., *in* "Proceedings, 7th Int. Symp-Reactivity of Solids, Bristol, 1972," p. 1. Chapman & Hall, London, 1972.